THE JOURNAL OF PHYSICAL CHEMISTRY C

Article

pubs.acs.org/JPCC

Asymmetric Organic–Inorganic Hybrid Giant Molecule: Cyanobiphenyl Monosubstituted Polyhedral Oligomeric Silsesquioxane Nanoparticles for Vertical Alignment of Liquid Crystals

Dae-Yoon Kim,[†] Soeun Kim,[†] Sang-A Lee,[†] Young-Eun Choi,[‡] Won-Jin Yoon,[†] Shiao-Wei Kuo,[§] Chih-Hao Hsu,[∥] Mingjun Huang,[∥] Seung Hee Lee,*[,‡] and Kwang-Un Jeong*[,†]

[†]Department of Polymer-Nano Science and Technology, Chonbuk National University, Jeonju 561-756, Korea

[‡]Department of BIN Fusion Technology, Chonbuk National University, Jeonju 561-756, Korea

[§]Department of Materials Science and Optoelectronic Engineering, National Sun Yat-Sen University, Kaohsiung 804, Taiwan

[∥]Department of Polymer Science, University of Akron, Akron, Ohio 44325, United States

Supporting Information

ABSTRACT: For liquid crystal (LC) alignment, polyhedral oligomeric silsesquioxanes (POSS) can be considered as one of the promising candidates for the formation of vertical alignment (VA) of LC. However, because of their poor compatibility and weak interaction with LC hosts, the pristine POSS are highly aggregate themselves in the LC media and create the macroscopic particles, resulting in severe light scatterings. To overcome this barrier, we proposed and successfully synthesized the cyanobiphenyl monosubstituted POSS giant molecule (abbreviated as POSS-CBP$_1$), which showed an excellent dispersion in nematic (N) LC media and formed the perfect VA of LC without using conventional polymer-based VA layers. On the basis of the systematic experiments and careful analysis, we realized that the cyanobiphenyl moiety chemically attached to the pristine POSS with an alkyl chain can significantly improve the initial solubility and interaction with LC media but finely tune POSS-CBP$_1$ to gradually diffuse onto the substrate of LC cell for the formation of VA layer without forming the macroscopic aggregations. Therefore, the newly developed POSS-CBP$_1$ VA layer can allow us to significantly cut the manufacturing cost as well as to open the new doors for electro-optical applications.

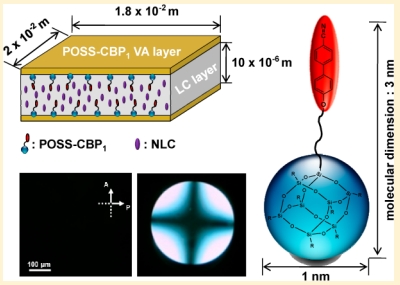

INTRODUCTION

Liquid crystal (LC) alignment has attracted considerable interests not only in scientific aspects of partially ordered soft materials but also in engineering point of views of LC displays (LCD).[1−4] Especially in LCD industry, the display engineers have developed many LC modes distinguished by the way of LC alignment, such as twisted nematic (TN),[5,6] vertical alignment (VA),[7−9] in-plane switching (IPS),[10] and fringe-field switching (FFS) mode.[11−13] Among them, the vertical LC alignment method has some advantages over the homogeneous planar LC alignment because the VA LC cells fabricated using the homeotropically oriented LC without an electric field exhibit better electro-optical performances, such as a high contrast, wide viewing angle, fast response time, and unnecessary mechanical rubbing process for the macroscopic LC alignment.[14−16]

In the VA LC mode, the long axes of the LC molecules are aligned parallel to the surface normal at the initial state. While a threshold voltage is applied, the long axes of the LC molecules reorient to horizontal direction with respect to the substrate.[17−21] It is well-known that the high contrast ratio of LCD should show a clear dark state without an electric field.[22,23] Therefore, the VA LCD requires a VA layer to make the homeotropic alignment of LC with respect to the substrate. The polyimide-type polymeric materials have been most widely used as the LC alignment layers. Recently, there are several reports for the modification of LC anchoring conditions on the surface of substrates by introducing lecithin, silanes, and carbon-based nanomaterials.[24−28]

Since the polymer-type alignment layer has many problems such as long process time, low yield, and high cost, the nanoparticle-induced VA of LC has been proposed recently due to the new electro-optical properties, such as memory effect, frequency modulation response, and low driving voltage.[29−34] Since the interaction between nanoparticles with substrates is higher than that between nanoparticles and LC compounds, the nanoparticles mixed with NLC hosts at the initial state can be phase-separated against the NLC media and diffused onto the substrates in which is a thermodynamically more stable state. The diffused and deposited nanoparticles on the substrates may form the VA of LC. Among many nanoparticles, polyhedral oligomeric silsesquioxanes (POSS) can be considered as one of

Received: December 26, 2013
Revised: February 28, 2014
Published: March 3, 2014

   dx.doi.org/10.1021/jp4126396 | J. Phys. Chem. C 2014, 118, 6300−6306

the promising candidates for the formation of VA of LC.[35] However, the first significant obstacle for the POSS application is the poor compatibility with LC media and the second is the weak interaction with LC molecules. Therefore, the pristine POSS are highly aggregated themselves in the LC media and create the macroscopic micrometer particles resulting in severe light scatterings.[36−42] To solve this problem, we proposed and successfully synthesized the cyanobiphenyl monosubstituted POSS giant molecule (abbreviated as POSS-CBP_1) in this research. POSS-CBP_1 showed an excellent dispersion in NLC media and formed the perfect VA of LC. From the experimental results, we concluded that the cyanobiphenyl group asymmetrically and chemically attached to the pristine POSS can improve the initial solubility and interaction with LC media but finely tune POSS-CBP_1 to diffuse to the substrates for the formation of VA layer without forming the macroscopic aggregations in the NLC bulk phase.

EXPERIMENTAL SECTION

Materials. 4-Cyano-4′-hydroxybiphenyl (CBP, 97%, Aldrich), ethyl 6-bromohexanoate (99%, Aldrich), aminopropylisobutyl POSS (POSS, Hybrid Plastics), triethylamine (TEA, 99%, Sigma-Aldrich), anhydrous *N,N*-dimethylformamide (DMF, 99.8%, Sigma-Aldrich), anhydrous tetrahydrofuran (THF, 99.9%, Sigma-Aldrich), absolute ethanol (EtOH, 99.5%, Sigma-Aldrich), acetone (99.9%, Samcheon Chemical), ethyl acetate (99.9%, Samcheon Chemical), chloroform (99.9%, Samcheon Chemical), hexanes (99.9%, Samcheon Chemical), thionyl chloride ($SOCl_2$, 90%, Daejung Chemical), hydrochloric acid (HCl, 37%, Sigma-Aldrich), potassium hydroxide (KOH, 95%, Showa), potassium carbonate (K_2CO_3, 99%, Showa), and nematic liquid crystal (MJ98468, Merck Co.) were used as received.

Synthesis of (4-Cyano-4′-biphenolxy)hexanoate Ethyl Ester (1). Ethyl 6-bromohexanoate (19.8 mL, 111 mmol) was attached to CBP (15.4 g, 78.9 mmol) in anhydrous DMF (100 mL) with anhydrous K_2CO_3 (10.8 g, 78.1 mmol) at 90 °C for 24 h. After reaction, resulting solution was filtered and dissolved in chloroform. Dissolved solution was extracted with water and then dried over $MgSO_4$. The product was recrystallized in ethanol (yield: 89%). ^{1}H NMR ($CDCl_3$, Figure S1): δ = 1.26 (t; 3H), 1.51 (m; 2H), 1.71 (m; 2H), 1.83 (m; 2H), 2.34 (t; 2H), 4.01 (t; 2H), 4.12 (q; 2H), 6.97 (d; 2H), 7.51 (d; 2H), 7.65 (m; 4H).

Synthesis of (4-Cyano-4′-biphenoxy)hexanoic Acid (2). A solution of **1** (2.05 g, 6.08 mmol) and KOH (3.6 g, 64.16 mmol) was stirred in the 150 mL of absolute ethanol and refluxed at 65 °C for 3 h. After cooling, the solution was poured into cold distilled water about 500 mL, and then, 1 M HCl (50 mL) was added to precipitate the acid product which was collected by filtration, washed with water and cold acetone, and dried in vacuo at 60 °C (yield: 98%). ^{1}H NMR (DMSO-*d*, Figure S2): δ = 1.45 (m; 2H), 1.61 (m; 2H), 1.74 (m; 2H), 2.23 (t; 2H), 4.01 (t; 2H), 7.02 (d; 2H), 7.64 (m; 4H), 7.92 (d; 2H), 11.6 (broad singlet; 1H).

Synthesis of POSS-CBP_1 (3). A solution of **2** (2.18 g, 7.10 mmol) was dissolved in 80 mL of $SOCl_2$ and refluxed at 70 °C for 5 h under a N_2 atmosphere. After reaction, organic solvent was removed in vacuum, and the remaining crude material was dissolved in 25 mL of anhydrous THF. A solution of aminopropylisobutyl POSS (5.12 g, 5.86 mmol) with TEA (2.24 mL, 5.86 mmol) in 25 mL of anhydrous THF was added into previous solution and stirred at room temperature overnight. After reaction, organic solvent was removed in vacuum, and the remaining residue was extracted with water, aqueous ammonia solution, and chloroform. The organic layer was dried over $MgSO_4$, and then it was purified by column chromatography with silica gel using ethyl acetate:chloroform = 1:1. Resulting product was white powder (yield: 80.5%). ^{1}H NMR ($CDCl_3$, Figure S3): δ = 0.59 (m; 16H), 0.94 (d; 42H), 1.51 (m; 2H), 1.71 (m; 2H), 1.85 (m; 11H), 2.20 (t; 2H), 3.24 (q; 2H), 4.01 (t; 2H), 5.44 (t; 1H), 6.97 (d; 2H), 7.51 (d; 2H), 7.65 (m; 4H). MALDI-ToF-MS (*m*/*z*): 1165.92 (calculated for $C_{50}H_{88}N_2O_{14}Si_8$); 1165.10 ($[M + H]^+$, observed).

One Drop Filling (ODF) Process. In our typical test LC cells were made by the filling process of NLC/POSS-CBP_1 mixtures between two glass substrates. Glass substrates were washed with distilled water, acetone, and isopropyl alcohol several times. Cleaned substrates were in a drying oven at 80 °C for 1 h. A series of NLC/POSS-CBP_1 (99.0/1.0, 99.7/0.3, 99.9/0.1, and 99.98/0.02 respectively) mixtures with the NLC and POSS-CBP_1 compound are prepared by heating up to 120 °C in the ultrasonic mixer for 10 min. After NLCs and POSS-CBP_1s are completely mixed, a certain concentration of NLC/POSS-CBP_1 mixtures were filled into glass capillary and then the mixtures were dropped on the surface of glass substrate on a 120 °C hot plate by using capillary reaction. After dropping the mixtures, the cells were covered and their cell gap was controlled to be 10 μm by applying a spacer.

Dipping Process. The monolayered organic−inorganic hybrid thin films for vertical alignment of NLC were prepared by dipping process of glass substrates in POSS-CBP_1 solution. The precleaned glass substrates were dipped in the 0.02 wt % of the POSS-CBP_1/acetone solution for 1 h. The POSS-CBP_1-coated substrates by the dipping method were slowly dried. Note that the dip-coated POSS-CBP_1 substrates were not much changed even after the mild rinsing with acetone, which result indicates that the once formed POSS-CBP_1 protrusions on the glass substrates are strong enough against chemical attacks. The LC cells were fabricated by filling the NLC between the POSS-CBP_1 treated substrates which were sandwiched by 10 μm cell gap.

Characterization. The thermal behavior of the POSS-CBP_1 giant molecule was monitored using a PerkinElmer PYRIS Diamond DSC equipped with an Intracooler 2P apparatus. The temperatures and heat flows were calibrated using standard materials at the cooling and heating rates of 10 °C/min. Heating scans always preceded the cooling scans at the same rate to eliminate the previous thermal histories. The transition temperatures were determined by measuring the onset temperatures obtained during the cooling and heating scans. The change of optical textures at a given temperature was observed using cross-polarized POM (Nikon ECLIPSE E600POL) coupled with a LINKAM LTS 350 heating stage. ^{1}H NMR spectra were recorded on a JNM-EX400 spectrometer. MALDI-ToF mass spectrometry has been performed using a Voyager-DE STR Biospectrometry Workstation. Contact angle was measured by contact angle analyzer (Phoenix-300, SEO). Atomic force microscopy images were recorded on an Agilent 550 AFM (Agilent Technologies) using silicon cantilevers with spring constants of 20−30 N/m. The resonance frequencies were set as 140−160 kHz, and the scan speed varied from 0.5 to 1.0 line/s.

dx.doi.org/10.1021/jp4126396 | J. Phys. Chem. C 2014, 118, 6300−6306

RESULTS AND DISCUSSION

VA Formation by Doping POSS-CBP$_1$ Giant Molecule.

As shown in Scheme 1, we newly designed and synthesized the novel asymmetric giant molecule (POSS-CBP$_1$) which was chemically connected with a cyanobiphenyl moiety by a flexible alkyl chain. Chemical structures and purity of POSS-CBP$_1$ and its intermediates were confirmed by thin layer chromatography (TLC), proton nuclear magnetic resonance (^{1}H NMR, Figures S1−S3 in the Supporting Information), and matrix-assisted laser desorption/ionization time-of-flight mass spectrometry (MALDI-ToF MS, Figure S4 in the Supporting Information). By chemically attaching the cyanobiphenyl mesogen to POSS nanoparticle with an alkyl chain connector, the compatibility and interaction of POSS-CBP$_1$ with LC compounds will be significantly increased. Indeed, the solubility of POSS-CBP$_1$ in common organic solvents, such as chloroform, acetone, and tetrahydrofuran, is dramatically enhanced compared with that of the pristine POSS. When the compatibility and interaction of POSS-CBP$_1$ with LC compounds are properly tuned by attaching the cyanobiphenyl mesogen and alkyl chain, we can expect that the initially dissolved POSS-CBP$_1$ in the NLC is gradually phase-separated from the NLC medium and diffused onto the substrate of LC cell without forming the macroscopic aggregations in the NLC bulk phase and then construct the POSS-CBP$_1$ monolayer which is an ideal surface structure for the formation of VA of LC.

To test this proposal, a series of NLC/POSS-CBP$_1$ mixtures with the NLC (MJ98468, Merck Co.) are prepared by heating up to 120 °C in the ultrasonic mixer for 10 min. The test LC cells were made by sandwiching the mixtures between two glass substrates. The cell gap is controlled to be 10 μm by applying spacer balls of 10 μm diameter. Here, the NLC/POSS-CBP$_1$ mixtures were filled into the LC cells on a 120 °C hot plate utilizing the one drop filling (ODF) process which method can prevent the flow effect and cooled down to room temperature at 10 °C/min. The macroscopic images of test LC cells are taken at room temperature by a digital camera (Nikon, Coolpix 995) with Polaroid films on top and bottom of the cell at a right angle with the respect to each other and the microscopic images of the LC cells are taken at room temperature from POM with transmissive mode. The VA of NLC is examined by the conoscopic observation with Bertrand lens. As shown in Figure 1, four different types of LC cells with 10 μm cell gap are prepared by varying the NLC/POSS-CBP$_1$ weight ratio from 99.0/1.0, 99.7/0.3, 99.9/0.1, to 99.98/0.02, respectively.

Scheme 1. Synthetic Procedure of POSS-CBP$_1$[a]

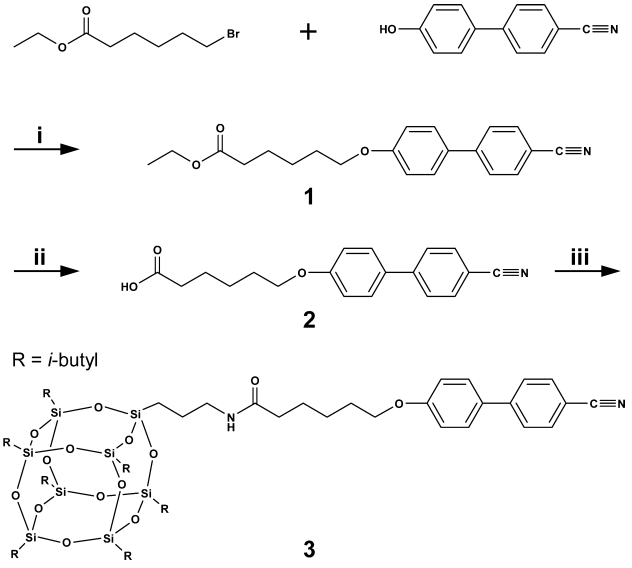

[a]Reagents and conditions: (i) DMF, K_2CO_3, 90 °C for 24 h; (ii) EtOH, KOH, 65 °C for 3 h; (iii) $SOCl_2$, 70 °C for 5 h under N_2 purge → POSS, TEA, THF, 25 °C for 15 h.

Nematic liquid crystal: MJ98468 (Merck Co.)

$\Delta\varepsilon$ = -4.0, Δn = 0.077 (at 589.3 nm), T_{NI} = 75 °C

POSS-CBP$_1$

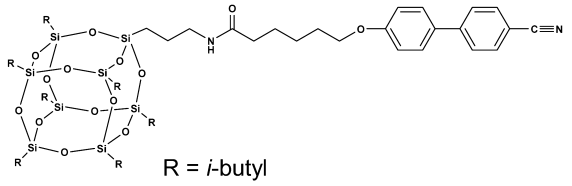

	Composition (wt%)			
POSS-CBP$_1$	1.0	0.3	0.1	0.02
MJ98468	99.0	99.7	99.9	99.98

Figure 1. Materials information: host nematic liquid crystal (NLC) MJ98468, POSS-CBP$_1$ molecule, and their weight ratio in the mixture.

The macroscopic images of the LC cells between the Polaroid films with 1.0, 0.3, and 0.1 wt % of POSS-CBP$_1$ in NLC are shown in Figure 2a−c, respectively, and their corresponding orthoscopic and conoscopic images of the VA of LC are also evaluated by POM (Figure 2d−f and insets, respectively). From the macroscopic image of Figure 2a, it is obvious that the macroscopic image of the LC cell with 1.0 wt % POSS-CBP$_1$ does not show any characteristics of vertical (homeotropic) alignment, but the randomly oriented multifold NLC domains. As shown in the inset of Figure 2d, there is no sign of the Maltese cross in the concoscopic POM image which is a direct evidence of the homeotropic alignment of the LC cell.[43−45] Note that the homeotropically aligned LC phase should exhibit a dark state under crossly equipped polarizer (two pieces of polarizers are arranged at a 90° angle with respect to each other) due to the fact that the molecular orientation of LC are aligned normal to the surface of test LC cell and do not exhibits any birefringence (zero birefringence effect).[46]

When the content of POSS-CBP$_1$ in the LC mixture is reduced from 1.0 to 0.3 wt % to prevent the aggregation of POSS-CBP$_1$ by themselves, the dark state area in the macroscopic image is significantly increased (Figure 2b) even though light leakages are still detected. The dark state in the magnified POM image (Figure 2e) and the Maltese cross in the conoscopic POM image (inset of Figure 2e) indicate that the homeotropic VA of LC is locally achieved. However, the birefringent LC domains in Figure 2e point out the fact that

dx.doi.org/10.1021/jp4126396 | J. Phys. Chem. C 2014, 118, 6300−6306

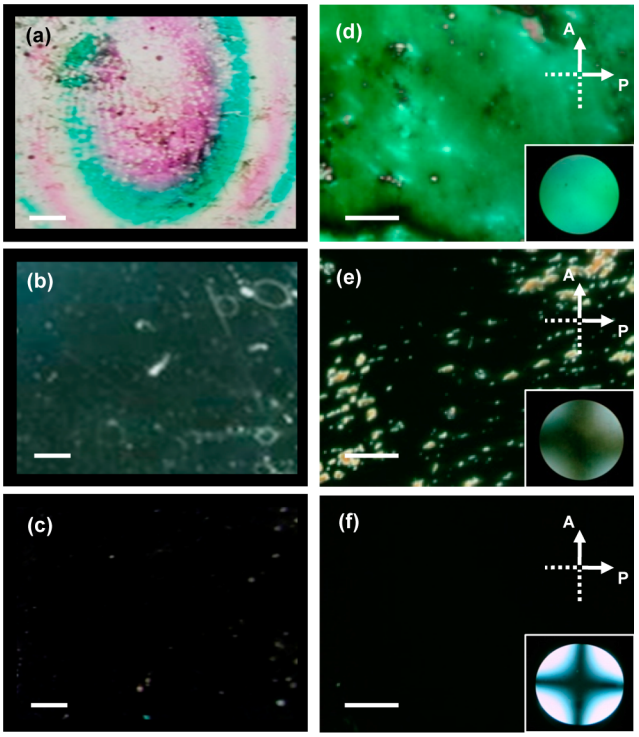

Figure 2. Macroscopic images (scale bar = 5 mm) (a–c) and their orthoscopic (scale bar = 100 μm) (d–f) and conoscopic (inset) POM images of the NLC/POSS-CBP$_1$ filled cell with a weight ratio of 99.0:1.0 (a, d), 99.7:0.3 (b, e), and 99.9:0.1 (c, f), respectively.

there are still a great amount of macroscopic POSS-CBP$_1$ aggregations in the LC cell. Note that the achievement of the homeotropic LC in the pristine POSS/NLC cell needs to be doped of large amount POSS more than 3.0 wt %, but it also causes aggregation problem which disturbs a perfect vertical alignment. If the content of POSS-CBP$_1$ is reduced even down to the 0.1 wt % in the NLC/POSS-CBP$_1$ mixture, the true dark state is obtained (Figure 2c,f), and the distinct Maltese cross (inset of Figure 2f) in the conoscopic POM images clearly represents the formation of the homeotropic VA of the NLC molecules.

VA Formation by Two-Dimensional Monolayered POSS-CBP$_1$ Protrusions. Even though the LC cell with the 0.1 wt % POSS-CBP$_1$ shows an excellent dark state, several small-size but large enough bright spots are detected as shown in the macroscopic image (Figure 2c). This result may come from the macroscopic aggregation of POSS-CBP$_1$ as well as from the uncovered substrates. Therefore, in order to create a uniform VA alignment layer with POSS-CBP$_1$, we need to control the concentration of POSS-CBP$_1$ in the LC mixture and the diffusion of POSS-CBP$_1$ onto the substrate. First, the theoretical compositions of POSS-CBP$_1$ for constructing the monolayer dispersion in LC cell with 20 mm × 18 mm (length and width) and 10 μm cell gap (height) should be calculated. Utilizing Cerius2 computer simulation software from Accelrys (version 4.6), the molecular dimension of POSS-CBP$_1$ is estimated, as illustrated in Figure 3a.[47−50] The calculated length of POSS-CBP$_1$ along the long axis is about 3 nm and short axis is 1 nm. It means that, from a rough calculation with specific assumptions, an ideal condition for monolayer dispersion of POSS-CBP$_1$ on sandwiched glass substrate with 10 μm cell gap is 0.02 wt %.

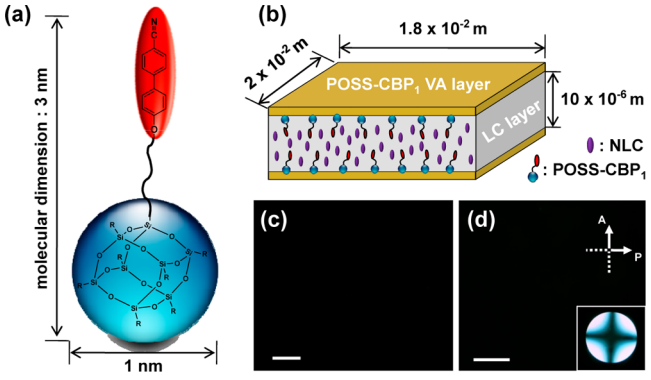

Figure 3. Calculated geometric dimension of POSS-CBP$_1$ molecule in the side view (a), schematic illustration of 0.02 wt % POSS-CBP$_1$ monolayer for vertical alignment induced test LC cell (b), macroscopic image (scale bar = 5 mm) (c), and POM image (scale bar = 100 μm) (d) of the test cell with 0.02 wt % POSS-CBP$_1$.

When the LC cell with the 0.02 wt % POSS-CBP$_1$ is fabricated by cooling the LC cell from 120 °C to the room temperature at 1 °C/min, a perfect dark state without any light leakage is obtained, as shown in Figure 3c,d. However, if the LC cell with the 0.02 wt % POSS-CBP$_1$ is rapidly cooled down, several bright spots are detected. This result represents the fact that the homogeneous POSS-CBP$_1$ monolayer may be created by optimizing the concentration of POSS-CBP$_1$ in the LC mixture and tuning the rates of phase separation from the NLC medium and diffusion of POSS-CBP$_1$ onto the substrates. Therefore, the formation of the uniform POSS-CBP$_1$ VA monolayer in the LC cell with the 0.02 wt % POSS-CBP$_1$ is also tested by a specifically designed experiment. The bare glass substrates are dipped in the 0.02 wt % of POSS-CBP$_1$/acetone solution for 1 h and acetone solvent on the substrates of the LC cell is slowly evaporated for 6 h. Because of a good solubility in organic solvents such as acetone, POSS-CBP$_1$ can be easily fabricated into films by a simple dipping process.

To investigate the uniform film-forming ability of POSS-CBP$_1$, the surface morphological investigation was carried out by atomic force microscopy (AFM). The surface of bare glass substrate were relatively smooth (Figure 4a). However, as shown in Figure 4b, the 0.02 wt % POSS-CBP$_1$ coated surface exhibited the many protrusions but constructed uniform continuous layer in each domain. The deionized (DI) water contact angle measurements of a bare glass substrate and a POSS-CBP$_1$ coated substrate also clearly indicate the fact that POSS-CBP$_1$ molecules are indeed on the glass substrate, as shown in Figure 5. The bare glass and 0.02 wt % POSS-CBP$_1$ coated glass substrate showed 28.8° (Figure 5a) and 39.6° (Figure 5b) of water contact angles, respectively, suggesting that hydrophobic layer was formed due to the hydrophobic cyanobiphenyl alkyl chains of the POSS-CBP$_1$. Note that the interaction between the POSS nanoparticle (silicon–oxygen cage structure) with glass substrates is much higher than between the cyanobiphenyl moieties and glass substrates. Thus, POSS-CBP$_1$ nanoparticles can be deposited with molecular orientation perpendicular to the surface of the glass substrate and formed the homeotropic alignment. The average width and height of protrusions of the POSS-CBP$_1$ layers (Figure 4c) are in the range of 62.5 and 2.41 nm, respectively, with the root-mean-square (RMS) surface roughness about 0.464 nm. Based on the AFM result, it is realized that two-dimensional (2D) monolayered POSS-CBP$_1$ protrusions are formed by the lateral

dx.doi.org/10.1021/jp4126396 | J. Phys. Chem. C 2014, 118, 6300–6306

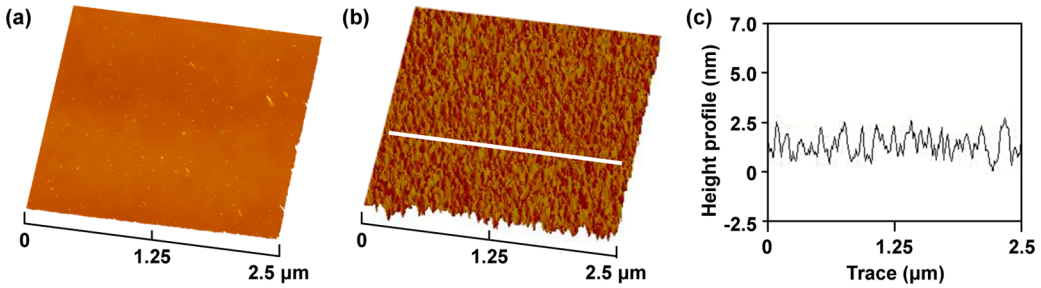

Figure 4. 3D topographic images of bare glass substrate (a), 0.02 wt % POSS-CBP_1 monolayer film on a glass substrate (b), and its height profile (c) along the white solid line in (b).

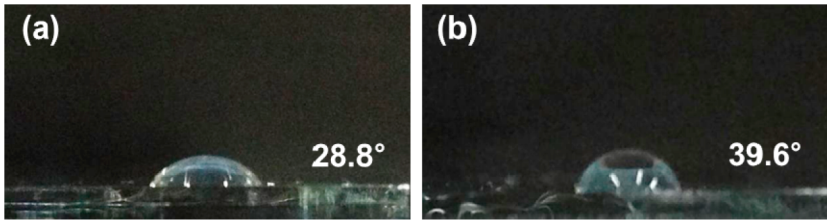

Figure 5. Contact angle measurements using distilled water images of bare glass substrate (a) and 0.02 wt % POSS-CBP_1 coated monolayer substrate (b).

self-assembly of POSS-CBP_1 giant molecules on the glass substrate. However, 0.02 wt % POSS-CBP_1 dip-coated substrates has a uniform continuous protrusion layer in each domain, but the average coated ratio of POSS-CBP_1 molecules on the surfaces is about 72.3%. Additionally, the cross section of CBP_1 group in POSS-CBP_1 giant molecule is roughly one-third of POSS group. Note that the calculated height and width of POSS-CB are 3 and 1 nm, respectively, based on the assumption of the *all-trans* conformation of alkyl chain (Figure 3a). Therefore, even though the POSS groups in POSS-CBP_1 are laterally close-packed and create the 2D monolayered protrusion domains, the tethered CBP_1 groups are mobile and provide the enough empty spaces for NLC to partially crawl into the empty zones and to stand up to create the first VA layer.

By using the dip-coated POSS-CBP_1 substrate, the LC cell fabricated by filling the NLC between the monodispersed POSS-CBP_1 treated substrates exhibits a perfect homeotropic VA of LC without any light scatterings at room temperature (Figure 6). In order to test the thermal stability of POSS-CBP_1 alignment layer, the temperature of the LC cell with the 0.02 wt % POSS-CBP_1 is increased up to the 75 °C (just below the T_{NI} transition temperature of NLC medium) and kept at 75 °C for 12 h. As shown in Figure 6, the homeotropic VA of LC is retained without any destruction of LC alignment. This result indicates that the once formed POSS-CBP_1 interaction with the substrates is strong enough to overcome the thermal fluctuations.

CONCLUSIONS

For liquid crystal (LC) alignment, POSS were first modified by chemically attaching the cyanobiphenyl moiety with a flexible alkyl chain connector. The POSS-CBP_1 asymmetric hybrid giant molecule exhibited an excellent dispersion in nematic (N) LC media and formed the perfect vertical alignment (VA) of LC without any light scatterings. From the systematic experiments of POSS-CBP_1 in NLC media, it was found that the cyanobiphenyl functional group chemically attached to the pristine POSS with an alkyl chain can significantly improve the compatibility with LC compounds but finely tune POSS-CBP_1 to gradually diffuse onto the substrate of LC cell for the formation of VA layer without forming the macroscopic aggregations.

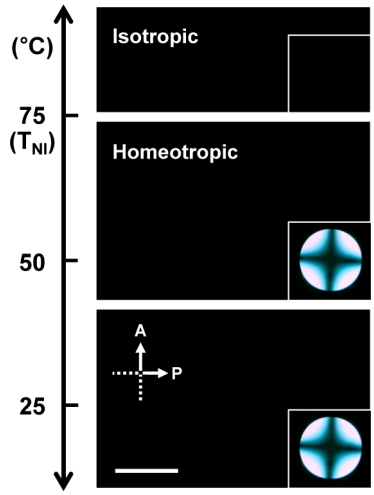

Figure 6. Thermal stabilities of 0.02 wt % POSS-CBP_1 dip-coated VA LC cell (scale bar = 100 μm).

ASSOCIATED CONTENT

Supporting Information

^{1}H NMR, MALDI-ToF MS, TGA, DSC, and detailed experimental procedures. This material is available free of charge via the Internet at http://pubs.acs.org.

AUTHOR INFORMATION

Corresponding Authors

*E-mail: kujeong@jbnu.ac.kr (K.-U.J.).
*E-mail: lsh1@jbnu.ac.kr (S.H.L.).

Notes

The authors declare no competing financial interest.

dx.doi.org/10.1021/jp4126396 | J. Phys. Chem. C 2014, 118, 6300−6306

■ ACKNOWLEDGMENTS

This work was mainly supported by Human Resource Training Project for Regional Innovation, Basic Science Research Program (2013R1A1A2007238), Converging Research Center Program (2013K000404), and BK21 Plus program, Korea. D.-Y. Kim appreciates the support from Global Ph.D. Fellowship Program (2013H1A2A1033907) and K.-U. Jeong acknowledges the support from LG Yonam Foundation.

■ REFERENCES

(1) Takatoh, K.; Hasegawa, M.; Koden, M.; Itoh, N.; Hasegawa, R.; Sakamoto, M. *Alignment Technologies and Applications of Liquid Crystal Devices*; Taylor & Francis Inc.: New York, 2005.

(2) Rasing, T.; Musevic, I. *Surfaces and Interfaces of Liquid Crystals*; Springer: New York, 2004.

(3) Hoogboon, J.; Garcia, P. M. L.; Otten, M. B. J.; Elemans, J. A. A. W.; Sly, J.; Lazarenko, S. V.; Rasing, T.; Rowan, A. E.; Nolte, R. J. M. Tunable Command Layers for Liquid Crystal Alignment. *J. Am. Chem. Soc.* **2005**, *127*, 11047−11052.

(4) Gin, D. L.; Lu, X.; Nemade, P. R.; Pecinovsky, C. S.; Xu, Y.; Zhou, M. Recent Advances in the Design of Polymerizable Lyotropic Liquid-Crystal Assemblies for Heterogeneous Catalysis and Selective Separations. *Adv. Funct. Mater.* **2006**, *16*, 865−878.

(5) Lee, S. H.; Bhattacharyya, S. S.; Jin, H. S.; Jeong, K.-U. Devices and Materials for High-Performance Mobile Liquid Crystal Displays. *J. Mater. Chem.* **2012**, *22*, 11893−11903.

(6) Lee, W.-K.; Choi, Y. S.; Kang, Y.-G.; Sung, J.; Seo, D.-S.; Park, C. Super-Fast Switching of Twisted Nematic Liquid Crystals on 2D Single Wall Carbon Nanotube Networks. *Adv. Funct. Mater.* **2011**, *21*, 3843−3850.

(7) Kang, Y. G.; Kim, H.-J.; Park, H.-.G.; Kim, B.-Y.; Seo, D.-S. Tin Dioxide Inorganic Nano-level Films with Different Liquid Crystal Molecular Orientations for Application in Liquid Crystal Displays (LCDs). *J. Mater. Chem.* **2012**, *22*, 15969−15975.

(8) Lu, R.; Wu, S.-T.; Lee, S. H. Reducing the Color Shift of a Multidomain Vertical Alignment Liquid Crystal Display Using Dual Threshold Voltages. *Appl. Phys. Lett.* **2008**, *92*, 0511141−051143.

(9) Zhou, J.; Collard, D. M.; Park, J. O.; Srinivasaro, M. Control of the Anchoring Behavior of Polymer-Dispersed Liquid Crystals: Effect of Branching in the Side Chains of Polyacrylates. *J. Am. Chem. Soc.* **2002**, *124*, 9980−9981.

(10) Oh-e, M.; Kondo, K. Response Mechanism of Nematic Liquid Crystals Using the In-plane Switching Mode. *Appl. Phys. Lett.* **1996**, *69*, 623−625.

(11) Lee, S. H.; Lee, S. L.; Kim, H. Y. Electro-optic Characteristics and Switching Principle of a Nematic Liquid Crystal Cell Controlled by Fringe-Field Switching. *Appl. Phys. Lett.* **1998**, *73*, 2881−2883.

(12) Yun, H. J.; Jo, M. H.; Jang, I. W.; Lee, S. H.; Ahn, S. H.; Hur, H. Jin. Achieving High Light Efficiency and Fast Response Time in Fringe Field Switching Mode using a Lliquid Crystal with Negative Dielectric Anisotropy. *Liq. Cryst.* **2012**, *39*, 1141−1148.

(13) Yu, I. H.; Song, I. S.; Lee, J. Y.; Lee, S. H. Intensifying the Density of a Horizontal Electric Field to Improve Light Efficiency in a Fringe-Field Switching Liquid Crystal Display. *J. Phys. D: Appl. Phys.* **2006**, *39*, 2367−2372.

(14) Hunter, J. T.; Pal, S. K.; Abbott, N. L. Adsorbate-Induced Ordering Transitions of Nematic Liquid Crystals on Surfaces Decorated with Aluminum Perchlorate Salts. *ACS Appl. Mater. Interfaces* **2010**, *2*, 1857−1865.

(15) Takeda, A.; Kataoka, S.; Sasaki, T.; Chida, H.; Tsuda, H.; Ohmuro, K.; Sasabayashi, T.; Koike, Y.; Okamoto, K. A Super-High Image Quality Multi-Domain Vertical Alignment LCD by New Rubbing-Less Technology. *SID Dig.* **1998**, *29*, 1077−1080.

(16) Xu, M.; Yang, D.-K.; Bos, P. J.; Jin, X.; Harris, F. W.; Cheng, S. Z. D. Very High Pretilt Alignment and Its Application in Pi-Cell LCDs. *SID Dig.* **1998**, *29*, 139−142.

(17) Schiekel, M. F.; Fahrenschon, K. Deformation of Nematic Liquid Crystals with Vertical Orientation in Electrical Fields. *Appl. Phys. Lett.* **1971**, *19*, 391−393.

(18) Geary, J. M.; Goodby, J. W.; Kmetz, A. R.; Patel, J. S. The Mechanism of Polymer Alignment of Liquid-Crystal Materials. *J. Appl. Phys.* **1987**, *62*, 4100−4108.

(19) Kim, S. G.; Kim, S. M.; Kim, Y. S.; Lee, H. K.; Lee, S. H.; Lee, G.-D.; Lee, J.-J.; Kim, K. H. Stabilization of the Liquid Crystal Director in the Patterned Vertical Alignment Mode through Formation of Pretilt Angle by Reactive Mesogen. *Appl. Phys. Lett.* **2007**, *90*, 261910−261913.

(20) Zhao, D.; Huang, W.; Cao, H.; Zheng, Y.; Wang, G.; Yang, Z.; Yang, H. Homeotropic Alignment of Nematic Liquid Crystals by a Photocross-Linkable Organic Monomer Containing Dual Photofunctional Groups. *J. Phys. Chem. B* **2009**, *113*, 2961−2965.

(21) Liu, B.-Y.; Chen, L.-J. Role of Surface Hydrophobicity in Pretilt Angle Control of Polymer-Stabilized Liquid Crystal Alignment Systems. *J. Phys. Chem. C* **2013**, *117*, 13474−13478.

(22) Yoshida, H. *Handbook of Visual Display Technology*; Springer: New York, 2005.

(23) Kim, J. B.; Lim, J. R.; Park, J. S.; Ahn, H. J.; Lee, M. J.; Jo, S. J.; Kim, M.; Kang, D.; Lee, S. J.; Kim, Y. S.; Baik, H. K. The Directional Peeling Effect of Nanostructured Rigiflex Molds on Liquid-Crystal Devices: Liquid-Crystal Alignment and Optical Properties. *Adv. Funct. Mater.* **2008**, *18*, 1340−1347.

(24) Hara, M.; Nagano, S.; Seki, T. π-π Interaction-Induced Vertical Alignment of Silica Mesochannels Templated by a Discotic Lyotropic Liquid Crystal. *J. Am. Chem. Soc.* **2010**, *132*, 13654−13656.

(25) Hwang, B. H.; Ahn, H. J.; Rho, S. J.; Chae, S. S.; Baik, H. K. Vertical Alignment of Liquid Crystals with Negative Dielectric Anisotropy on an Inorganic Thin Film with a Hydrophilic Surface. *Langmuir* **2009**, *25*, 8306−8312.

(26) Weiss, K.; Woll, C.; Bohm, E.; Fiebranz, B.; Forstmann, F.; Peng, B.; Scheumann, V.; Johannsmann, D. Molecular Orientation at Rubbed Polyimide Surfaces Determined with X-ray Absorption Spectroscopy: Relevance for Liquid Crystal Alignment. *Macromolecules* **1998**, *31*, 1930−1936.

(27) Hahm, S. G.; Lee, T. J.; Chang, R.; Jung, J. C.; Zin, W.-C.; Ree, M. Unusual Alignment of Liquid Crystals on Rubbed Films of Polyimides with Fluorenyl Side Groups. *Macromolecules* **2006**, *39*, 5385−5392.

(28) Noonan, P. S.; Shavit, A.; Acharya, B. R.; Schwartz, D. K. Mixed Alkylsilane Functionalized Surfaces for Simultaneous Wetting and Homeotropic Anchoring of Liquid Crystals. *ACS Appl. Mater. Interfaces* **2011**, *3*, 4374−4380.

(29) Bisoyi, H. K.; Kumar, S. Liquid-Crystal Nanoscience: An Emerging Avenue of Soft Self-Assembly. *Chem. Soc. Rev.* **2011**, *40*, 306−319.

(30) Park, H.-G.; Lee, J.-J.; Dong, K.-Y.; Oh, B.-Y.; Kim, Y.-H.; Jeong, H.-Y.; Ju, B.-K.; Seo, D.-S. Homeotropic Alignment of Liquid Crystals on a Nano-patterned Polyimide Surface using Nanoimprint Lithography. *Soft Matter* **2011**, *7*, 5610−5614.

(31) Wang, X.; Wang, H.; Luo, L.; Huang, J.; Gao, J.; Liu, X. Dependence of Pretilt Angle on Orientation and Conformation of Side Chain with Different Chemical Structure in Polyimide Film Surface. *RSC Adv.* **2012**, *2*, 9463−9472.

(32) Glushchenko, A.; Kresse, H.; Reshetnyak, V.; Qeznikov, Y. U.; Yaroshshuk, O. Memory Effect in Filled Nematic Liquid Crystals. *Liq. Cryst.* **1997**, *23*, 241−246.

(33) Shiraishi, Y.; Toshima, N.; Meada, K.; Yoshikawa, H.; Xu, J.; Kobayashi, S. Frequency Modulation Response of a Liquid-crystal Electro-optic Device Doped with Nanoparticles. *Appl. Phys. Lett.* **2002**, *81*, 2845−2847.

(34) Lee, W.; Wang, C.-Y.; Shih, Y.-C. Effects of Carbon Nanosolids on the Electro-optical Properties of a Twisted Nematic Liquid-crystal Host. *Appl. Phys. Lett.* **2004**, *85*, 513−515.

(35) Kuo, S.-W.; Chang, F.-C. POSS Related Polymer Nanocomposites. *Prog. Polym. Sci.* **2011**, *36*, 1649−1696.

(36) Qi, H.; Hegmann, T. Impact of Nanoscale Particles and Carbon Nanotubes on Current and Future Generations of Liquid Crystal Displays. *J. Mater. Chem.* **2008**, *18*, 3288−3294.
(37) Goodby, J. W.; Saez, I. M.; Cowling, S. J.; Gortz, V.; Draper, M.; Hall, A. W.; Sia, S.; Cosquer, G.; Lee, S.-E.; Raynes, E. P. Transmission and Amplification of Information and Properties in Nanostructured Liquid Crystals. *Angew. Chem., Int. Ed.* **2008**, *47*, 2754−2787.
(38) Kumar, S.; Pal, S. K.; Kumar, P. S.; Lakshminarayanan, V. Novel Conducting Nanocomposites: Synthesis of Triphenylene-covered Gold Nanoparticles and Their Insertion into a Columnar Matrix. *Soft Matter* **2007**, *3*, 896−900.
(39) Yu, X.; Yue, K.; Hsieh, I.-F.; Li, Y.; Dong, X.-H.; Liu, C.; Xin, Y.; Wang, H.-F.; Shi, A.-C.; Newkome, G. R.; Ho, R.-M.; Chen, E.-Q.; Zhang, W.-B.; Cheng, S. Z. D. Giant Surfactants Provide a Versatile Platform for Sub-10-nm Nanostructure Engineering. *Proc. Natl. Acad. Sci. U. S. A.* **2013**, *110*, 10078−10083.
(40) Patra, A.; Chandaluri, C. G.; Radhakrishnan, T. P. Optical Materials Based on Molecular Nanoparticles. *Nanoscale* **2012**, *4*, 343−359.
(41) Li, Y.; Zhang, W.-B.; Hsieh, I.-F.; Zhang, G.; Cao, Y.; Li, X.; Wesdemiotis, C.; Lotz, B.; Xiong, H.; Cheng, S. Z. D. Breaking Symmetry toward Nonspherical Janus Particles Based on Polyhedral Oligomeric Silsesquioxanes: Molecular Design, "Click" Synthesis, and Hierarchical Structure. *J. Am. Chem. Soc.* **2011**, *133*, 10712−10715.
(42) Sun, H.-J.; Tu, Y.; Wang, C.-L.; Van Horn, R. M.; Tsai, C. C.; Graham, M. J.; Sun, B.; Lotz, B.; Zhang, W.-B.; Cheng, S. Z. D. Hierarchical Structure and Polymorphism of a Sphere-cubic Shape Amphiphile based on a Polyhedral Oligomeric Silsesquioxane-[60]fullerene Conjugate. *J. Mater. Chem.* **2011**, *21*, 14240−14247.
(43) Lockwood, N. A.; de Pablo, J. J.; Abbott, N. L. Influence of Surfactant Tail Branching and Organization on the Orientation of Liquid Crystals at Aqueous-Liquid Crystal Interfaces. *Langmuir* **2005**, *21*, 6805−6814.
(44) Yasuda, T.; Shimizu, T.; Liu, F.; Ungar, G.; Kato, T. Electro-Functional Octupolar π-Conjugated Columnar Liquid Crystals. *J. Am. Chem. Soc.* **2011**, *133*, 13437−13444.
(45) Seltmann, J.; Marini, A.; Mennucci, B.; Dey, S.; Kumar, S.; Lehmann, M. Nonsymmetric Bent-Core Liquid Crystals based on a 1,3,4-Thiadiazole Core Unit and Their Nematic Mesomorphism. *Chem. Mater.* **2011**, *23*, 2630−2636.
(46) Dierking, I. *Textures of Liquid Crystals*; Wiley-VCH: Weinheim, 2003.
(47) Kim, D.-Y.; Lee, S.-A; Choi, H. J.; Chien, L.-C.; Lee, M.-H.; Jeong, K.-U. Reversible Actuating and Writing Behaviours of a Head-to-Side Connected Main-Chain Photochromic Liquid Crystalline Polymer. *J. Mater. Chem. C* **2013**, *1*, 1375−1382.
(48) Kim, N.; Wang, L.; Kim, D.-Y.; Hwang, S.-H.; Kuo, S.-W.; Lee, M.-H.; Jeong, K.-U. Macroscopically Oriented Hierarchical Structure of the Amphiphilic Tetrathiafulvalene Molecule. *Soft Matter* **2012**, *8*, 9183−9192.
(49) Kim, D.-Y.; Wang, L.; Cao, Y.; Yu, X.; Cheng, S. Z. D.; Kuo, S.-W.; Song, D.-H.; Lee, S. H.; Jeong, K.-U. The Biaxial Lamello-columnar Liquid Crystalline Structure of a Tetrathiafulvalene Sanidic Molecule. *J. Mater. Chem.* **2012**, *22*, 16382−16389.
(50) Park, S.-K.; Kim, S.-E.; Kim, D.-Y.; Kang, S.-W.; Shin, S.; Kuo, S.-W.; Hwang, S.-H.; Lee, S. H.; Lee, M.-H.; Jeong, K.-U. Polymer-Stabilized Chromonic Liquid-Crystalline Polarizer. *Adv. Funct. Mater.* **2011**, *21*, 2129−2139.